Inorganic Chemistry

Article

pubs.acs.org/IC

Spacer-Directed Selective Assembly of Copper Square or Hexagon and Ring-Stacks or Coordination Nanotubes

Xialu Wu,[†] Nini Ding,[‡] Wenhua Zhang,[‡] Fei Xue,[†] and T. S. Andy Hor*[,†,‡]

[†]Department of Chemistry, Faculty of Science, National University of Singapore, 3 Science Drive 3, 117543, Singapore

[‡]Institute of Materials Research & Engineering, Agency for Science, Technology & Research, 3 Research Link, 117602, Singapore

Supporting Information

ABSTRACT: The use of simple self-assembly methods to direct or engineer porosity or channels of desirable functionality is a major challenge in the field of metal−organic frameworks. We herein report a series of frameworks by modifying square ring structure of $[\{Cu_2(5\text{-dmpy})_2(L_1)_2(H_2O)(MeOH)\}_2\{ClO_4\}_4]\cdot 4MeOH$ (**1**·4MeOH, 5-dmpy = 5,5′-dimethyl-2,2′-bipyridine, HL_1 = 4-pyridinecarboxylic acid). Use of pyridyl carboxylates as directional spacers in bipyridyl chelated Cu(II) system led to the growth of square unit into other configurations, namely, square ring, square chain, and square tunnel. Another remarkable characteristic is that the novel use of two isomers of pyridinyl−acrylic acid directs selectively to two different extreme tubular forms—aligned stacking of discrete hexagonal rings and crack-free one-dimensional continuum polymers. This provides a unique example of two extreme forms of copper nanotubes from two isomeric spacers. All of the reactions are performed in a one-pot self-assembly process at room temperature, while the topological selectivity is exclusively determined by the skeletal characteristics of the spacers.

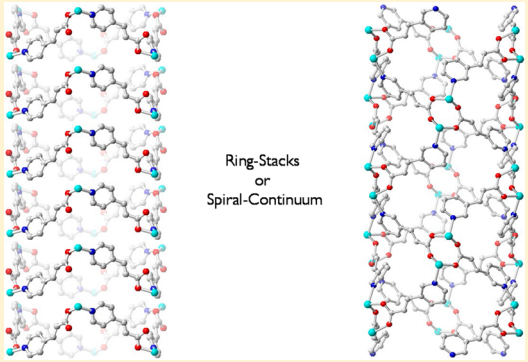

INTRODUCTION

Metal−organic frameworks (MOFs) and related supramolecular assemblies are new materials of rich potential in selective gas sorption, solute transport and delivery, shape-directed nanosynthesis, small molecule and ion exchanges, etc.[1] Among the synthetic methods developed for these materials, the most common one is spontaneous self-assembly of metals and spacers.[1g,2] Since the porosity or channel characteristics can be adjusted by the spacer dimension and the functional groups it carries,[3] a major challenge in self-assembly is the use of this simple way to direct or engineer channels of desirable shape, porosity, and morphology.[4] One of the best-known MOF systems is assembled by carboxylate ligands in taking advantage of their diverse coordination modes.[5] Continuous interests in these modified MOF systems are on carboxylate-based hybrid ligands that would lead to diverse functional MOFs.[6]

Encouraged by these and as part of our continual investigations on pyridyl carboxylate hybrid ligands,[7] we herein report the self-assembly of pyridyl carboxylates with Cu(II) in giving five new MOFs with different configurations (Chart 1). First, we isolated three MOFs based on square unit, that is, square ring (**1**), square chain (**2**), and square tunnel (**3**), supported by an ancillary bipyridyl, in a one-pot self-assembly process. CO_2 sorption analysis of these three materials revealed that the highly packing tubular structure **3** showed the highest CO_2 adsorption capacity. Encouraged by this finding, we subsequently designed and constructed another two tubular structures, by modifying the ligands used in **3**. This approach demonstrated that two isomers of pyridinyl−acrylic acid could yield a common hexagonal ring but two different material forms—stacking of discrete rings and intertwine of 1D spirals. The self-assembly of polygonal conduits of two extreme forms, namely, aligned stacking of polygons and intertwine of 1D polymers, in giving continuum and "crack-free" channels represents a convenient and powerful entry to molecular materials of desirable features. There are many examples of the stacked form,[6a,8] but much less is known on the continuum relative.[9] There is also no simple ligand system that can direct to both forms through self-assembly. All the five materials are synthesized under ambient conditions from the solutions of $Cu(ClO_4)_2\cdot 6H_2O$, bipyridyl chelate, and pyridyl carboxylate linkers. This discovery of an unusually simple method with readily available synthons fuels the optimism that designed assembly of polygonal frameworks or conduits ("coordination nanotube") of targeted morphological features is within sight.

EXPERIMENTAL SECTION

All chemicals used in the synthesis were of reagent grade from commercial sources and used as received. Elemental analyses were performed on a PerkinElmer PE 2400 elemental analyzer. Thermogravimetric analyses (TGA) were performed on TA Instruments SDT 2960 Simultaneous DTA-TGA equipment from room temperature (r.t.) to 1000 °C under N_2 atmosphere at a heating rate of 10 °C·min^{-1}. Infrared spectra were recorded on the Varian 3100 FT-IR spectrometer using KBr pellets. Powder X-ray diffraction (PXRD) spectra were recorded on Bruker D8 General Area Detector

Received: October 21, 2014
Published: June 30, 2015

DOI: 10.1021/ic502552y
Inorg. Chem. 2015, 54, 6680−6686

Chart 1. Ligands for the Construction of Frameworks

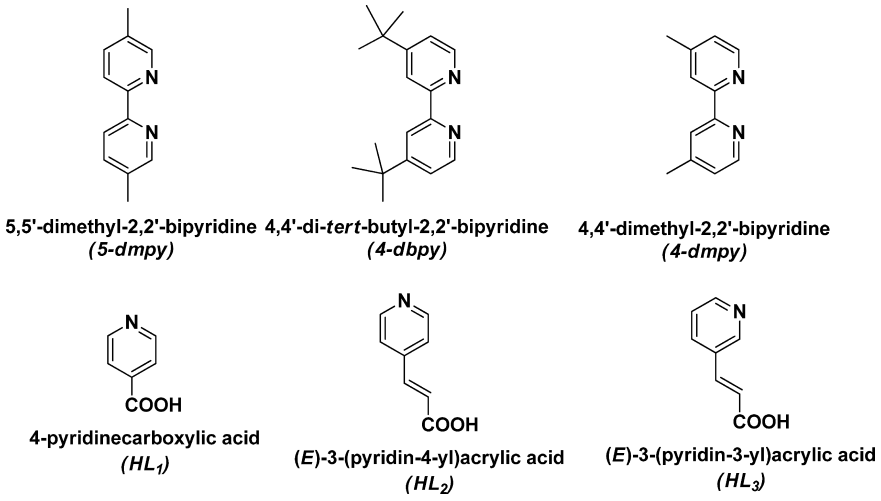

Diffraction System (GADDS) XRD microdiffractometer equipped with a VANTEC-2000 area detector with Φ rotation method. The X-ray generated from a sealed Cu tube was monochromated by a graphite crystal and collimated by a 0.5 mm MONOCAP (λ Cu Kα = 1.541 78 Å). The tube voltage and current were 40 kV and 40 mA. Gas sorption isotherms were measured with a Micromeritics ASAP 2020 Surface Area and Porosity Analyzer. An oven-dried sample tube equipped with a TranSeal (Micromeritics) was weighed. The sample was transferred into the sample tube, which was then capped by a TranSeal. The sample was heated to 120 °C under a vacuum of 2 mTorr for 16 h. The evacuated sample tube was weighed again, at which point the outgas rate was less than 2 mTorr/min, and the sample mass was determined by subtracting the mass of the previously weighed tube. The N_2 and CO_2 isotherms were measured using a liquid nitrogen bath (77 K) and dry ice/acetone (195 K), respectively. ***Caution!*** *$Cu(ClO_4)_2{\cdot}6H_2O$ is explosive and should be handled with care!*

Preparation of 1. A solution of 5,5′-dimethyl-2,2′-bipyridine (18.4 mg, 0.10 mmol) in CH_2Cl_2 (5 mL) was added to the solution of $Cu(ClO_4)_2{\cdot}6H_2O$ (36.9 mg, 0.10 mmol) in MeOH (5 mL) dropwise with stirring. The solution was further stirred at ambient temperature for half an hour. A solution of isonicotinic acid (12.3 mg, 0.10 mmol) in MeOH (5 mL) was then subsequently added dropwise. The resultant clear solution was stirred at ambient temperature for another half an hour and then filtered. The clear filtrate was allowed to stand at ambient temperature for a few days to provide blue crystals, which were filtered, washed with MeOH, and dried in air. Yield: 36.5 mg, 74%. Anal. Calcd (%) for $C_{75.5}H_{79}Cl_7Cu_4N_{12}O_{28}$: C 43.08, H 3.78, N 7.99; found C 42.95, H 3.55, N 8.26%.

Preparation of 2. **2** was synthesized using a similar procedure as that of **1** but using 4,4′-di-*tert*-butyl-2,2′-bipyridine (26.8 mg, 0.10 mmol) in MeOH (5 mL), $Cu(ClO_4)_2{\cdot}6H_2O$ (36.9 mg, 0.10 mmol) in MeOH (5 mL) and (*E*)-3-(pyridin-4-yl)acrylic acid (14.9 mg, 0.10 mmol) in MeOH (5 mL) instead. **2** was isolated as blue crystals, washed with MeOH, and further air-dried prior to elemental analysis. Yield: 37.0 mg, 64%. Anal. Calcd (%) for $C_{104}H_{152}Cl_4Cu_4N_{12}O_{40}$: C 47.93, H 5.88, N 6.45; found C 47.52, H 6.12, N 6.32%.

Preparation of 3. **3** was synthesized using a similar procedure as that of **1** but using 5,5′-dimethyl-2,2′-bipyridine (18.4 mg, 0.10 mmol) in EtOH (5 mL), $Cu(ClO_4)_2{\cdot}6H_2O$ (36.9 mg, 0.10 mmol) in H_2O (5 mL), and (*E*)-3-(pyridin-3-yl)acrylic acid (14.9 mg, 0.10 mmol) in H_2O (5 mL) instead. **3** was isolated as blue crystals, washed with H_2O and EtOH, and further air-dried prior to elemental analysis. Yield: 34.0 mg, 69%. Anal. Calcd (%) for $C_{80}H_{88}Cl_4Cu_4N_{12}O_{32}$: C 45.20, H 4.17, N 7.91; found C 45.04, H 4.36, N 8.18%.

Preparation of 4. **4** was synthesized using a similar procedure as that of **1** but using 5,5′-dimethyl-2,2′-bipyridine (18.4 mg, 0.10 mmol) in EtOH (5 mL), $Cu(ClO_4)_2{\cdot}6H_2O$ (36.9 mg, 0.10 mmol) in H_2O (5 mL), and (*E*)-3-(pyridin-4-yl)acrylic acid (14.9 mg, 0.10 mmol) in H_2O (5 mL) instead. **4** was isolated as blue crystals, washed with H_2O and EtOH, and further air-dried prior to elemental analysis. Yield: 33.0 mg, 64%. Anal. Calcd (%) for $C_{120}H_{150}Cl_6Cu_6N_{18}O_{57}$: C 43.02, H 4.51, N 7.52; found C 43.15, H 4.29, N 7.44%.

Preparation of 5. **5** was synthesized using a similar procedure as that of **1** but using 4,4′-dimethyl-2,2′-bipyridine (18.4 mg, 0.10 mmol) in EtOH (5 mL), $Cu(ClO_4)_2{\cdot}6H_2O$ (36.9 mg, 0.10 mmol) in H_2O (5 mL), and (*E*)-3-(pyridin-3-yl)acrylic acid (14.9 mg, 0.10 mmol) in H_2O (5 mL) instead. **5** was isolated as blue crystals, washed with H_2O and EtOH, and further air-dried prior to elemental analysis. Yield: 37.0 mg, 75%. Anal. Calcd (%) for $C_{120}H_{156}Cl_6Cu_6N_{18}O_{60}$: C 42.33, H 4.62, N 7.41; found C 42.48, H 4.24, N 7.52%.

X-ray Crystallography. The crystallographic measurements were performed on a Bruker SMART CCD diffractometer for **1** and **3**−**5** at 100 K and a Bruker APEX II for **2** at 123 K. The two instruments were both equipped with graphite-monochromated Mo Kα radiation (λ = 0.710 73 Å). The program SMART[10] was used for collecting frames, indexing reflections, and determining lattice parameters, SAINT for integration of the intensity of reflections and scaling, SADABS[11] for absorption correction, and SHELXTL[12] for space group and structure determination and least-squares refinements on F^2. The relevant crystallographic data and refinement details are shown in Supporting Information. The region of disordered electron density was removed from the structure, and the data were treated with the SQUEEZE routine in PLATON.[13]

RESULTS AND DISCUSSION

Mixing three solutions, namely, $Cu(ClO_4)_2{\cdot}6H_2O$ in MeOH, 5,5′-dimethyl-2,2′-bipyridine (5-dmpy) in CH_2Cl_2, and 4-pyridinecarboxylic acid (HL_1) in MeOH in a single reaction pot at r.t. resulted, upon workup, in the isolation of a blue solid formulated as $[\{Cu_2(5\text{-dmpy})_2(L_1)_2(H_2O)(MeOH)\}_2\{ClO_4\}_4]{\cdot}4MeOH$ (**1**·4MeOH). X-ray single-crystal crystallographic analysis revealed a Cu(II) metallo-square. The four copper atoms in the ring are bridged by L_1 ligand with a head-to-tail arrangement, using its monodentate carboxylate oxygen and pyridyl nitrogen donors (∠O1−Cu1−N2 89.42(9)°, ∠O3A−Cu2−N1 87.75(9)°; Figure 1a). The four Cu(II) centers within the metallomacrocycle are positioned within the same plane (deviation of 0.000 Å). A chelating bipyridyl at the equatorial position and an axial O atom (O5 from MeOH and O6 from H_2O) completes a distorted square pyramidal geometry of Cu(II).

The cation of **1** is assembled as a macrocycle with +4 charge. The electronic neutrality is met by perchlorate anions outside the metallosupramolecular cavity and at the intersection of four

DOI: 10.1021/ic502552y
Inorg. Chem. 2015, 54, 6680−6686

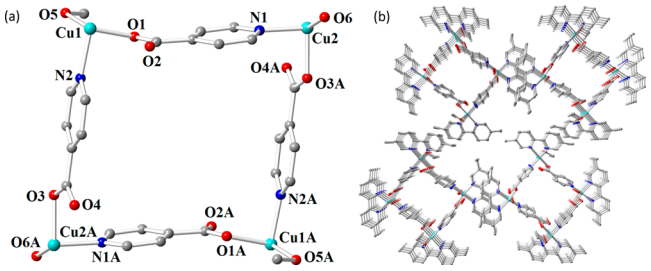

Figure 1. Framework of **1** showing (a) cationic square with coordinated H_2O and MeOH, the bipyridyl and hydrogen atoms are removed, and (b) stacked and aligned quadrangular conduit. Symmetry code: A $-x + 1, -y, -z + 2$.

connecting squares (Figure S2, Supporting Information). The four Cu(II) atoms are divided into two sets (Cu1 and Cu2; Figure 1a) coordinated with MeOH (O5) and H_2O (O6), respectively. This difference is amplified in the two slightly unequal sides of the square (8.84 and 8.76 Å, denoting the Cu···Cu distances). The higher steric effect of MeOH is manifested in weak $\pi-\pi$ interactions[14] between the neighboring bipyridyls at Cu1, while significant $\pi-\pi$ interactions between those at Cu2 (distance between two neighboring bipyridyls of 3.41 Å) were observed.

The bipyridyl serves two key functions—to provide a shield on each copper to prohibit secondary coordination to give three-dimensional network and to provide the axis for $\pi-\pi$ contact whereby individual quadrangular cupro-macrocycle rings can be stacked and aligned. This intermolecular interaction is strengthened by H-bonding between the aqua (O6) and neighboring carboxylates (O4A′) (H6X···O4A′ 1.977 Å; ∠O6−H6X-O4A′ 156.4°; Figure S3, Supporting Information). They collectively help to juxtapose the rings to stack upon each other to give a quadrangular conduit (Figure 1b). This is different from the most common pyridyl-based square ring in which the $\pi-\pi$ interactions between pyridyl rings are central to conduit formation.[15]

To clarify the relationship between the ligands used and the construction outcome, we optimized the ligands used in **1** and successfully isolated another two materials based on square units, namely, **2** and **3**. Replacing 5-dmpy by more bulky supporting ligand 4,4′-di-*tert*-butyl-2,2′-bipyridine (4-dbpy) and HL_1 by longer spacer HL_2 ((*E*)-3-(pyridin-4-yl)acrylic acid) leads to the isolation of $[Cu_4(4\text{-dbpy})_4(L_2)_4(ClO_4)_4]_n$ (**2**). Replacement of L_1 by HL_3 ((*E*)-3-(pyridin-3-yl)acrylic acid) in the synthesis gives $[\{Cu_2(5\text{-dmpy})_2(L_3)_2\}_2\{ClO_4\}_4]_n \cdot 3n(EtOH)$ (**3**·*n*EtOH) with a square tunnel structure.

Similar to **1**, the four copper atoms in each repeating ring of **2** and **3** are connected by a singly bridging L_2/L_3 ligand with a head-to-tail arrangement using its monodentate carboxylate oxygen and pyridyl nitrogen donors (Figure 2c,d). In **2**, a chelating bipyridyl and O atoms from H_2O (O1W and O1WA)/μ-O type carboxylate (O2 and O2A) completes a

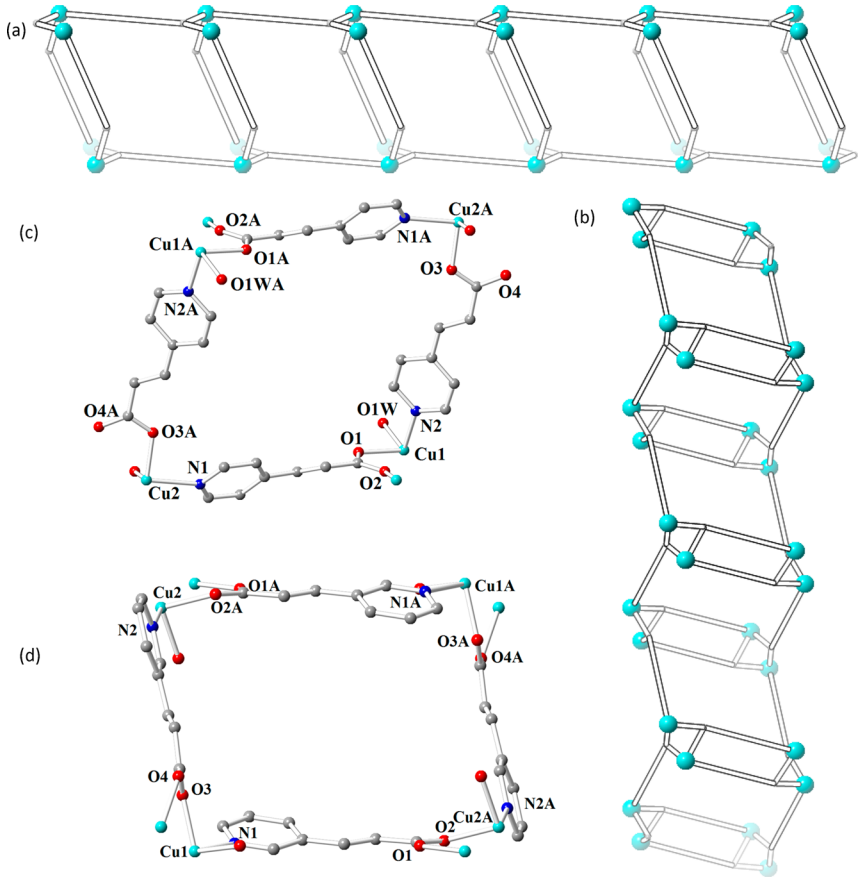

Figure 2. (a) Framework of **2** showing side topological view of the continuum of the stair-stepping chain; (b) framework of **3** showing side topological view of the continuum of the nanotube; (c) repeating square unit of **2** with the coordination mode of the Cu center (bipyridyl ligands are omitted), and (d) repeating square unit of **3** with the coordination mode of the Cu center (bipyridyl ligands are omitted). Symmetry codes: A $-x + 2, -y + 2, -z$ (**2**); A $x, -y, z + 1/2$ (**3**).

DOI: 10.1021/ic502552y
Inorg. Chem. 2015, 54, 6680−6686

distorted square pyramidal geometry (Figure S5, Supporting Information). With μ-O carboxylate donor, it resulted in a stair-stepping chain by a continuum of discrete Cu_4 square ring (9.97 × 10.84 $Å^2$, measured between the Cu centers; Figure 2a). In **3**, a conduit lined by a continuum of square pyramidal Cu2 interconnected by bridging carboxylate and terminal pyridyl is evident (Figure 2b). The electroneutrality of the compound is maintained by the presence of perchlorate anions located inside and in-between the square structures of **2** and **3** (Figures S7 and S12, Supporting Information), which resembles that found in **1**.

The change of the nitrogen disposition from 4- (or *para*- in HL_2) to 3- (or *meta*- in HL_3) position with respect to the acrylate alters the direction of polymeric propagation from horizontal (in **2**) to diagonal (in **3**), thus allowing four orthogonal points of interconnection in every Cu_2 node in **3**. This resulted in a novel matrix of continuum spirals that define the wall of the nanoconduit with a side-to-side distance of 11.44 × 9.04 $Å^2$. The $\pi-\pi$ interaction[14] between bipyridyl ligands (plane distance 3.66 Å; centroid distance 4.42 Å) of neighboring channels adds strength to the tubular network (Figure S11, Supporting Information). The steric effect of *tert*-butyl group in HL_2 does not support $\pi-\pi$ interactions between bipyridyl ligands, and there is no other significant interaction found between neighboring chains in **2**, resulting in chains that are independent from each other (Figure S6, Supporting Information).

Another remarkable characteristic is that the novel use of two isomers of pyridinyl–acrylic acid direct selectively to two different extreme tubular forms—aligned stacking of discrete hexagonal rings, **4** (Figure 3a), and crack-free 1D continuum

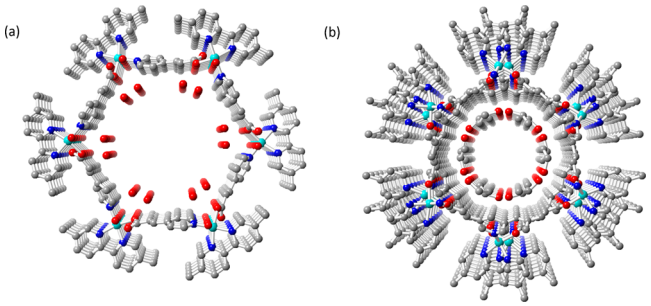

Figure 3. (a) Top view of **4** showing a water channel within a macrocyclic stack-sheet structure. (b) Top view of **5** showing hexagonally packed EtOH molecules within a nanotubular structure.

polymers, **5** (Figure 3b). Mix of three solutions, namely, $Cu(ClO_4)_2·6H_2O$ in H_2O, 5-dmpy in EtOH, and HL_2 in H_2O in a one-pot reaction at r.t. resulted, upon workup, in the isolation of a blue crystal formulated as $[\{Cu(5\text{-dmpy})(L_2)(H_2O)\}\{ClO_4\}]_6·15H_2O$ (**4**·$15H_2O$). X-ray single-crystal crystallographic analysis revealed a hexacationic and hexagonal Cu(II) metallomacrocycle (diagonal Cu···Cu 20.30 Å) in which the six copper atoms are connected in a ring by a singly bridging L_2 using its monodentate carboxylate oxygen and pyridyl nitrogen donors (∠O–Cu–N 90.79 (9)°). The six Cu(II) centers within a metallomacrocycle are uniformly positioned below and above the central plane with the deviation of 2.6241 Å (Figure 4a). An equatorial chelating bipyridyl and axial aqua (O1W) completes a distorted square pyramidal geometry (Figure S13, Supporting Information). Replacement of 5-dmpy by 4-dmpy and L_2 by L_3 in the

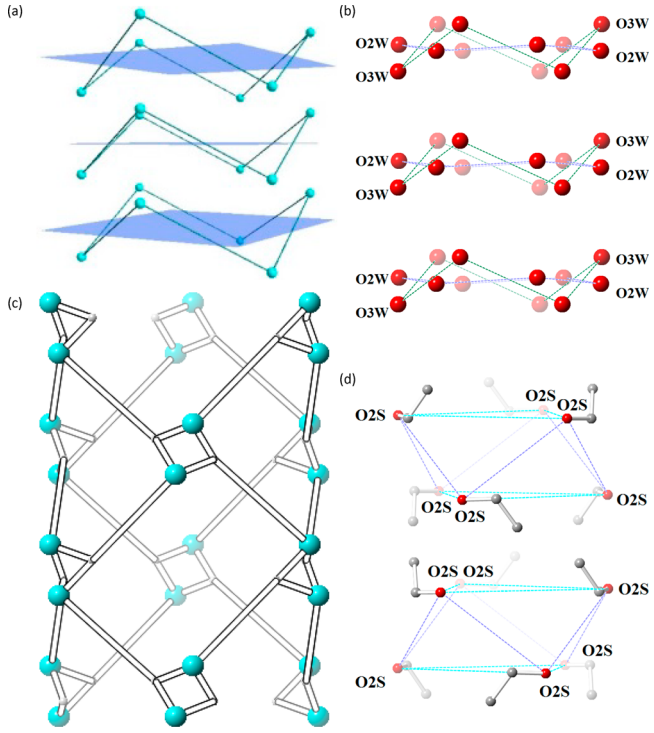

Figure 4. Side view of **4** showing (a) the chair-like formation of the copper hexagons; (b) two sets of crystallographically unique water molecules assembled in form of intercalation of a flattened hexagonal oxygen (O2W) ring (green) and a chairlike oxygen (O3W) ring (purple); (c) side topological view of **5** showing the connectivity of nanotube among the Cu2 nodes and the carboxylate ligands, and (d) crystallographically unique EtOH molecules located within the nanotubular structure, forming double triangle layer hexagonal rings (blue-green dotted line shows the triangle layer, and purple dotted line shows the hexagonal chair configurations, respectively).

synthesis gives a different material $[\{Cu(4\text{-dmpy})(L_3)\}\{ClO_4\}]_{6n}·2n$EtOH (**5**·2*n*EtOH) whose X-ray crystallographic analysis gave a conduit lined by a continuum of square pyramidal Cu_2 interconnected by bridging carboxylate and terminal pyridyl.

Similar to **1**, the $\pi-\pi$ interaction between bipyridyls and H-bonding between the aqua and neighboring carboxylates collectively help to juxtapose the individual hexagonal cupromacrocycle rings to stack upon each other (distance between two neighboring bipyridyls 6.942 Å) to give a hexagonal conduit with secondary aqua filling the void to give a water channel (Figures 3a and 4b). The effect of the change of the nitrogen disposition from 4- (or *para*- in HL_2) to 3- (or *meta*- in HL_3) position was also found in **5**, which allows four orthogonal points of interconnection in every Cu_2 node (Figure 4c), resulting in a matrix of continuum spirals (Figure 3b) that define the wall of the nanoconduit with a side-to-side distance of 15.46 Å. The $\pi-\pi$ interaction between bipyridyl ligands (3.46 Å) of neighboring rings adds strength to the tubular network (Figure S18, Supporting Information). In both **4** and **5**, the perchlorate anions are located outside the metallo-supramolecular cavity but at the intersection of three of the connecting nanotubular structures (Figures S14 and S17, Supporting Information).

Each cupro-macrocyclic cavity of **4** contains 12 secondary hydrate molecules arranged as an intercalation of a nearly flattened sheet of six aqua oxygen (O2W) with a chair of six

DOI: 10.1021/ic502552y
Inorg. Chem. 2015, 54, 6680–6686

oxygen (O3W), each with half occupancy (Figure 4b). A large portion of spatially delocalized electron density in the inner sphere of the channel was found, but its refinement did not give definitive results. A total of 271 electrons were found in each cell, which may suggest additional 27 H_2O molecules. These 27 water molecules correspond to 9 H_2O for each Cu_6 unit (Z = 3). The O2W and O3W separation of 2.350(15) Å (∠O3W−H1W3−O2W 130.2°) suggests H-bonding between the two water rings. The primary aqua (O1W) molecules are not pointed toward the center of the cavity, thus limiting their participation in H-bonding with the secondary aqua in the channel. Short separations between the coordinated carboxylate O atoms (O1) and the channel water (O2W) (O2W···O1 2.736(3) Å; ∠O2W−H2W2−O1 167.8°) suggest additional hydrogen bonding between the secondary water and the carboxylate ligands. The distance between O2W and O3W is 2.350(15) Å, which also makes the H-bonding between O2W and O3W possible (O3W···O2W 2.350(15) Å; ∠O3W−H1W3−O2W 130.2°). This is reminiscent of the water molecules in single-walled carbon nanotubes.[6a] This hydrate channel is related but different from the most common polymorph of ice, namely, hexagonal ice I (ice I_h),[16] which consists of sheets of tessellating hexamers in chair conformations linked together through an extensive H-bonding network (average O−H···O distance of 2.75 Å and H−O−H angle of 109° for ice I_h).

The EtOH solvate in **5** are evenly distributed inside and in-between the tubular cavity. The symmetry-equivalent positions of the Cu2 node suggests that the EtOH solvates inside the tubular cavity form double triangle layer hexagonal rings with chair configurations (Figure 4d). Unlike **4**, there is no obvious H-bonding among the EtOH in the channel, which is somewhat surprising.

To differentiate the thermal stability of the five materials, we performed TGA under a nitrogen gas flow. All of these five materials are thermally stable up to ~225−280 °C (**1**, ~280 °C; **2**, ~245 °C; **3**, ~255 °C; **4**, ~225 °C; **5**, ~245 °C; Figure 5

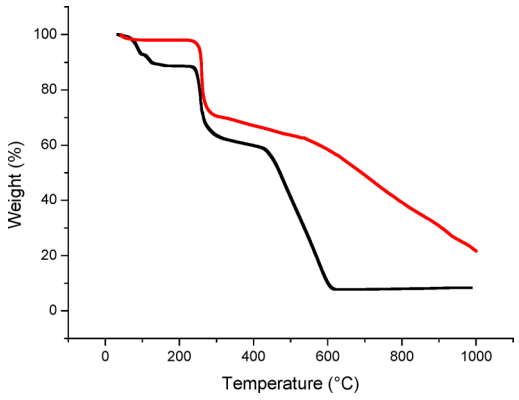

Figure 5. TGA profiles of **4** (black) and **5** (red).

and Figures S19−S21, Supporting Information). Figure 5 shows the thermogravimetric curves of **4** and **5**. In **4**, the initial mass loss from 34 °C corresponds to the complete removal of the crystalline water molecules, whereas the weight loss from ~110 °C is due to the loss of coordination water. From ~250 °C, the organic constituents disintegrate. The water extrusion pattern is similar to that of other related inorganic materials and topological structures.[17] According to the formula obtained from single-crystal XRD, **4**·15H_2O is [{Cu(5-dmpy)(L_2)-(H_2O)}{ClO_4}]$_6$·15H_2O; the observed weight drop due to water loss (~12%) is consistent with the calculated loss of ~11% (primary hydrate of 3% + secondary hydrate of 8%). The initial solvate loss in **5** is consistent with the two sets of EtOH found in and between the cavities. Notably, because of the explosive property of perchlorate, these complexes should be handled with care, and the TGA profiles may take an abrupt dive. Grinding small quantities of these samples into fine powder for our cases provides a solution to this issue.

Gas sorption studies were made on these five materials. All frameworks show significantly higher selectivity of CO_2 over N_2. The Brunauer−Emmett−Teller (BET) surface areas calculated from N_2 sorption data for **1**−**5** suggest that these frameworks are not active toward N_2 even at 77 K. This may be explained by the 1D channels that prevent effective N_2 diffusion; in other words, the channels are not open pores.[18] However, the sorption of CO_2 at low pressures and 195 K is notable (Figure 6 and Figures S22−S25, Supporting

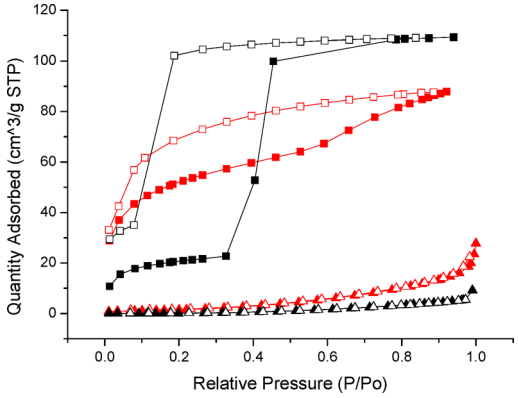

Figure 6. CO_2 absorption (■) and desorption (□) isotherms (195 K) and N_2 absorption (▲) and desorption (△) isotherms (77 K) measured for **4** (red) and **5** (black).

Information), which revealed a type IV behavior typical for microporous materials with hysteresis between sorption/desorption curves.[19] As mentioned above, the tubular structure (**3**) shows higher overall CO_2 uptake capacity (59.1 $cm^3 \cdot g^{-1}$), while the maximum capacities of another two square structures are ~12.3 (**1**) and 28.9 $cm^3 \cdot g^{-1}$ (**2**), respectively (Figure S25, Supporting Information). The different gas sorption behaviors of these three materials suggest the influence of spacers on both topology and porosity. In addition, the capacity of **4** and **5** shows up to 87 (**4**) and 109 $cm^3 \cdot g^{-1}$ (**5**) (3.92 and 4.88 $mmol \cdot g^{-1}$ at standard temperature and pressure, respectively). This is comparable to the reported carboxylate- and phosphonate-based MOFs reported by Zhou et al. and Costantino et al.[20] In addition, different from the other four materials **1**−**4**, a gating pressure at ~250 mmHg was found in **5**, resulting in abrupt changes in the sorption isotherms of CO_2. The continuum nature of the nanotube in **5** is probably responsible for its higher uptake and retention of the gases. Their stronger sorption of CO_2 over N_2 suggests the advantage of using the polarity of the carboxylate groups to attract small molecules with quadrupolar moments such as CO_2.[20a,21] Possible H-bonding between CO_2 and H-bearing group at the conduit may also contribute to the selectivity toward CO_2.[21b] It is notable that the powder pattern changed dramatically after the gas sorption. This might be caused by the structural change or structural destruction upon activation.

DOI: 10.1021/ic502552y
Inorg. Chem. 2015, 54, 6680−6686

CONCLUSIONS

Self-assembly of pyridyl carboxylates with $Cu(ClO_4)_2$ and bipyridyls has produced two sets of related but distinctive forms of coordinative frameworks and nanotubes. This study demonstrated that a straight to obtuse change in the relative donor orientation and length of the spacer is sufficient to guide the assembly from a ring stack to a continuum nanotube to a continuum ring chain. This is achieved by changing from a horizontal 4- (or *para*-) to 3- (or *meta*-) polymeric propagation. A crack-free structure is achieved through multipoint orthogonal interconnections of metals and spacers. Their different structural forms are manifested in different affinity toward solvates (especially water versus ethanol channels of **4** and **5**) and their sorption affinity toward CO_2. Their production from simple one-step and one-pot spacer-driven self-assembly methodology offers a distinct advantage over other engineering materials. Their water stability offers an additional incentive for these materials to be used in applications such as flue gas sorption and cleansing. This paves a forward path in tuning of materials porosity through molecular engineering of spacers.

ASSOCIATED CONTENT

Supporting Information

X-ray crystallographic data and files in CIF format, atomic coordination, detailed structure description, plots of gas adsorption versus pressure, powder XRD patterns, TGA, and IR. The Supporting Information is available free of charge on the ACS Publications website at DOI: 10.1021/ic502552y.

AUTHOR INFORMATION

Corresponding Author

*E-mail: andyhor@nus.edu.sg.

Notes

The authors declare no competing financial interest.

ACKNOWLEDGMENTS

We acknowledge A*STAR, NUS and GSK (R-143-000-426-305) for financial support and crystallographic assistance from Hong Yimian and Tan Geok Kheng.

REFERENCES

(1) (a) Czaja, A. U.; Trukhan, N.; Muller, U. *Chem. Soc. Rev.* **2009**, *38*, 1284−1293. (b) Li, J.-R.; Sculley, J.; Zhou, H.-C. *Chem. Rev.* **2011**, *112*, 869−932. (c) Zhang, J.-P.; Zhang, Y.-B.; Lin, J.-B.; Chen, X.-M. *Chem. Rev.* **2011**, *112*, 1001−1033. (d) Ferey, G. *Chem. Soc. Rev.* **2008**, *37*, 191−214. (e) Dincă, M.; Yu, A. F.; Long, J. R. *J. Am. Chem. Soc.* **2006**, *128*, 8904−8913. (f) Ma, S.; Simmons, J. M.; Yuan, D.; Li, J.-R.; Weng, W.; Liu, D.-J.; Zhou, H.-C. *Chem. Commun.* **2009**, 4049−4051. (g) Li, B.; Chen, S.-W.; Chen, Z.; Chen, J.; Guo, J.-Z.; Liu, L. *CrystEngComm* **2011**, *13*, 6610−6612.

(2) (a) Sun, S.-S.; Silva, A. S.; Brinn, I. M.; Lees, A. J. *Inorg. Chem.* **2000**, *39*, 1344−1345. (b) Lehn, J.-M. *Angew. Chem., Int. Ed.* **1990**, *29*, 1304−1319. (c) Sekiya, R.; Nishikiori, S.-i.; Ogura, K. *J. Am. Chem. Soc.* **2004**, *126*, 16587−16600. (d) Northrop, B. H.; Yang, H.-B.; Stang, P. J. *Chem. Commun.* **2008**, 5896−5908. (e) Mahata, K.; Frischmann, P. D.; Würthner, F. *J. Am. Chem. Soc.* **2013**, *135*, 15656−15661. (f) Gütz, C.; Hovorka, R.; Klein, C.; Jiang, Q.-Q.; Bannwarth, C.; Engeser, M.; Schmuck, C.; Assenmacher, W.; Mader, W.; Topić, F.; Rissanen, K.; Grimme, S.; Lützen, A. *Angew. Chem., Int. Ed.* **2014**, *53*, 1693−1698. (g) Zhou, X.-P.; Liu, J.; Zhan, S.-Z.; Yang, J.-R.; Li, D.; Ng, K.-M.; Sun, R. W.-Y.; Che, C.-M. *J. Am. Chem. Soc.* **2012**, *134*, 8042−8045. (h) Xiao, X.-Q.; Jia, A.-Q.; Lin, Y.-J.; Jin, G.-X. *Organometallics* **2010**, *29*, 4842−4848.

(3) (a) Zhao, D.; Yuan, D.; Sun, D.; Zhou, H.-C. *J. Am. Chem. Soc.* **2009**, *131*, 9186−9188. (b) Furukawa, H.; Kim, J.; Plass, K. E.; Yaghi, O. M. *J. Am. Chem. Soc.* **2006**, *128*, 8398−8399. (c) Yaghi, O. M.; O'Keeffe, M.; Ockwig, N. W.; Chae, H. K.; Eddaoudi, M.; Kim, J. *Nature* **2003**, *423*, 705−714. (d) Deng, H.; Grunder, S.; Cordova, K. E.; Valente, C.; Furukawa, H.; Hmadeh, M.; Gándara, F.; Whalley, A. C.; Liu, Z.; Asahina, S.; Kazumori, H.; O'Keeffe, M.; Terasaki, O.; Stoddart, J. F.; Yaghi, O. M. *Science* **2012**, *336*, 1018−1023. (e) Eubank, J. F.; Mouttaki, H.; Cairns, A. J.; Belmabkhout, Y.; Wojtas, L.; Luebke, R.; Alkordi, M.; Eddaoudi, M. *J. Am. Chem. Soc.* **2011**, *133*, 14204−14207. (f) Furukawa, H.; Go, Y. B.; Ko, N.; Park, Y. K.; Uribe-Romo, F. J.; Kim, J.; O'Keeffe, M.; Yaghi, O. M. *Inorg. Chem.* **2011**, *50*, 9147−9152.

(4) Blau, W. J.; Fleming, A. J. *Science* **2004**, *304*, 1457−1458.

(5) (a) Zhang, Z.; Li, B.; Meng, X.; Yin, X.; Zhang, T. *Dalton Trans.* **2013**, *42*, 4306−4312. (b) Furukawa, H.; Ko, N.; Go, Y. B.; Aratani, N.; Choi, S. B.; Choi, E.; Yazaydin, A. Ö.; Snurr, R. Q.; O'Keeffe, M.; Kim, J.; Yaghi, O. M. *Science* **2010**, *329*, 424−428. (c) Affronte, M.; Carretta, S.; Timco, G. A.; Winpenny, R. E. P. *Chem. Commun.* **2007**, 1789−1797. (d) Danjo, H.; Hirata, K.; Noda, M.; Uchiyama, S.; Fukui, K.; Kawahata, M.; Azumaya, I.; Yamaguchi, K.; Miyazawa, T. *J. Am. Chem. Soc.* **2010**, *132*, 15556−15558.

(6) (a) Unruh, D. K.; Gojdas, K.; Libo, A.; Forbes, T. Z. *J. Am. Chem. Soc.* **2013**, *135*, 7398−7401. (b) Zhang, S.; Li, Y.; Liu, Y.; Cao, R.; Sun, C.; Ji, H.; Liu, S. *J. Mol. Struct.* **2009**, *920*, 284−288. (c) Ishiwata, T.; Furukawa, Y.; Sugikawa, K.; Kokado, K.; Sada, K. *J. Am. Chem. Soc.* **2013**, *135*, 5427−5432. (d) Madalan, A. M.; Paraschiv, C.; Sutter, J.-P.; Schmidtmann, M.; Müller, A.; Andruh, M. *Cryst. Growth Des.* **2004**, *5*, 707−711.

(7) (a) Teo, P.; Koh, L. L.; Hor, T. S. A. *Chem. Commun.* **2007**, 4221−4223. (b) Teo, P.; Hor, T. S. A. *Coord. Chem. Rev.* **2011**, *255*, 273−289. (c) Teo, P.; Koh, L. L.; Hor, T. S. A. *Dalton Trans.* **2009**, 5637−5646.

(8) (a) Sumida, K.; Brown, C. M.; Herm, Z. R.; Chavan, S.; Bordiga, S.; Long, J. R. *Chem. Commun.* **2011**, *47*, 1157−1159. (b) Bloch, E. D.; Murray, L. J.; Queen, W. L.; Chavan, S.; Maximoff, S. N.; Bigi, J. P.; Krishna, R.; Peterson, V. K.; Grandjean, F.; Long, G. J.; Smit, B.; Bordiga, S.; Brown, C. M.; Long, J. R. *J. Am. Chem. Soc.* **2011**, *133*, 14814−14822. (c) McDonald, T. M.; Lee, W. R.; Mason, J. A.; Wiers, B. M.; Hong, C. S.; Long, J. R. *J. Am. Chem. Soc.* **2012**, *134*, 7056−7065. (d) Kong, G.-Q.; Ou, S.; Zou, C.; Wu, C.-D. *J. Am. Chem. Soc.* **2012**, *134*, 19851−19857.

(9) (a) Panda, T.; Kundu, T.; Banerjee, R. *Chem. Commun.* **2012**, *48*, 5464−5466. (b) Luo, T.-T.; Wu, H.-C.; Jao, Y.-C.; Huang, S.-M.; Tseng, T.-W.; Wen, Y.-S.; Lee, G.-H.; Peng, S.-M.; Lu, K.-L. *Angew. Chem., Int. Ed.* **2009**, *48*, 9461−9464. (c) Wu, G.; Bai, J. Q.; Jiang, Y.; Li, G. H.; Huang, J.; Li, Y.; Anson, C. E.; Powell, A. K.; Qiu, S. L. *J. Am. Chem. Soc.* **2013**, *135*, 18276−18279. (d) Tseng, T. W.; Luo, T. T.; Su, C. C.; Hsu, H. H.; Yang, C. I.; Lu, K. L. *CrystEngComm* **2014**, *16*, 2626−2633.

(10) *SMART and SAINT Software Reference Manuals, Version 5.611;* Bruker Analytical X-Ray Systems, Inc.: Madison, WI, 2000.

(11) Sheldrick, G. M. *SADABS, Program for empirical absorption correction of area detector data;* University of Göttingen: Germany, 1996.

(12) (a) Sheldrick, G. M. *SHELX97 programs for the solution and refinement of crystal structures;* University of Göttingen: Germany, 1997. (b) Sheldrick, G. M. *Acta Crystallogr., Sect. A* **2008**, *64*, 112−122.

(13) (a) Spek, A. *J. Appl. Crystallogr.* **2003**, *36*, 7−13. (b) van der Sluis, P.; Spek, A. L. *Acta Crystallogr., Sect. A* **1990**, *46*, 194−201.

(14) Janiak, C. *J. Chem. Soc., Dalton Trans.* **2000**, 3885−3896.

(15) (a) Fujita, M.; Kwon, Y. J.; Washizu, S.; Ogura, K. *J. Am. Chem. Soc.* **1994**, *116*, 1151−1152. (b) Fujita, M.; Sasaki, O.; Mitsuhashi, T.; Fujita, T.; Yazaki, J.; Yamaguchi, K.; Ogura, K. *Chem. Commun.* **1996**, 1535−1536.

(16) Mascal, M.; Infantes, L.; Chisholm, J. *Angew. Chem., Int. Ed.* **2006**, *45*, 32−36.

(17) Zhao, B.; Cheng, P.; Chen, X.; Cheng, C.; Shi, W.; Liao, D.; Yan, S.; Jiang, Z. *J. Am. Chem. Soc.* **2004**, *126*, 3012−3013.

DOI: 10.1021/ic502552y
Inorg. Chem. 2015, 54, 6680−6686

(18) (a) Chen, S.-S.; Chen, M.; Takamizawa, S.; Wang, P.; Lv, G.-C.; Sun, W.-Y. *Chem. Commun.* **2011**, *47*, 4902−4904. (b) Jin, N.; Seo, J.; Hong, K.; Chun, H. *Microporous Mesoporous Mater.* **2012**, *150*, 32−37.
(19) (a) Zhang, Z.-X.; Ding, N.-N.; Zhang, W.-H.; Chen, J.-X.; Young, D. J.; Hor, T. S. A. *Angew. Chem., Int. Ed.* **2014**, *53*, 4628−4632. (b) Dybtsev, D. N.; Chun, H.; Yoon, S. H.; Kim, D.; Kim, K. *J. Am. Chem. Soc.* **2003**, *126*, 32−33. (c) Kanoo, P.; Matsuda, R.; Sato, H.; Li, L.; Jeon, H. J.; Kitagawa, S. *Inorg. Chem.* **2013**, *52*, 10735−10737.
(20) (a) Taddei, M.; Costantino, F.; Ienco, A.; Comotti, A.; Dau, P. V.; Cohen, S. M. *Chem. Commun.* **2013**, *49*, 1315−1317. (b) Li, J.-R.; Zhou, H.-C. *Nat. Chem.* **2010**, *2*, 893−898.
(21) (a) Dey, R.; Haldar, R.; Maji, T. K.; Ghoshal, D. *Cryst. Growth Des.* **2011**, *11*, 3905−3911. (b) Planas, N.; Dzubak, A. L.; Poloni, R.; Lin, L.-C.; McManus, A.; McDonald, T. M.; Neaton, J. B.; Long, J. R.; Smit, B.; Gagliardi, L. *J. Am. Chem. Soc.* **2013**, *135*, 7402−7405.

DOI: 10.1021/ic502552y
Inorg. Chem. 2015, 54, 6680−6686